Journal of Power Sources 223 (2013) 259–267

Contents lists available at SciVerse ScienceDirect

Journal of Power Sources

journal homepage: www.elsevier.com/locate/jpowsour

Thermal Impedance Spectroscopy - A method for the thermal characterization of high power battery cells

Matthias Fleckenstein [a,*], Sebastian Fischer [b], Oliver Bohlen [a], Bernard Bäker [c]

[a] BMW Peugeot Citroën Electrification GmbH, Taunusstraße 41, 80807 München, Germany
[b] Technische Universität Darmstadt, Fachgebiet Fahrzeugtechnik, 64287 Darmstadt, Germany
[c] Dresden University of Technology, Department of Vehicle Mechatronics, Institute of Automotive Engineering, 01069 Dresden, Germany

HIGHLIGHTS

- Thermal Impedance Spectroscopy is used for thermal characterization of battery cells.
- Transfer function of thermal battery model is developed and fitted to TIS results.
- Heat capacity and radial heat conductivity of cylindrical Li-ion cell are determined.
- Results of TIS and of conventional thermal characterization verifies the TIS.

ARTICLE INFO

Article history:
Received 5 December 2011
Received in revised form
27 July 2012
Accepted 31 July 2012
Available online 7 September 2012

Keywords:
Thermal Impedance Spectroscopy
Battery modeling
Thermal characterization
Heat conductivity measurement

ABSTRACT

A new approach of Thermal Impedance Spectroscopy (TIS) is introduced for thermal characterization of battery cells. It examines the transfer behavior between internal heat generation and resulting battery surface temperature in the frequency domain. Compared to previously published TIS methods the internal heat generation forced by electrical operation can be determined without any previous knowledge or assumptions on the electric/electrochemical behavior of the battery cell. The complete procedure is demonstrated by the TIS-application on a cylindrical High-Power Li-Ion cell. By the use of a thermal battery model, its theoretical transfer function can be fitted to the TIS-measurement results in the Nyquist-Plot. Consequently, the specific heat capacity and the heat conductivity of the cell's jelly roll can be derived. A comparison of the exemplary operated TIS to conventional thermal characterization methods shows a difference of 5% in the heat capacity and 12% in the heat conductivity determination. Future improvements on the experimental setup are suggested in order to reach a higher measurement accuracy and additionally, the systematic advantages of the easy to operate and non-destructive TIS-method are presented.

1. Introduction

Within the development process of automotive electrical energy storages, thermal–electrical cell simulations are used in multiple variations and simulation aims. Especially with growing battery cell sizes and increasing power demands, local temperature differences inside Li-ion cells may rise up to 10 °C and above. Thus internal battery temperatures more and more decouple from temperatures measured on the surface of a battery cell. Thus, battery aging or safety examinations that equate surface temperatures with a mean or maximum jelly roll temperature operate with a growing prediction error.

As a consequence, thermal battery simulation of high energy and high power Li-ion cells has become an important issue to predict temperature maximums and thermal gradients inside the battery. A thermal–electrical battery simulation model consists of a thermal heat dissipation model, an electrical/electrochemical cell model and their conjunction, a heat generation model.

Modeling and parameterization of electrical and electrochemical models are discussed extensively in literature (e.g. [5,10,17,21]). Thermal modeling approaches are generally based on Finite Difference [8], Finite Volume [6] or Finite Element Method [11,19] solving the Fourier's law of heat conductivity combined with convective [16] and/or radiative [15] heat transfer boundary conditions. One of the dominant sources of inaccuracy of the complete thermal–electrical model is the parameterization of the heat dissipation model.

Here, it is important to determine on one hand the anisotropic heat conduction behavior of the cell's internal jelly roll and on the other hand its specific heat capacity. In several studies of literature (e.g. [14,20]) previously published values of the thermal

* Corresponding author. Tel.: +49 176 601 14063.
E-mail address: Matthias.Fleckenstein@bpc-electrification.com (M. Fleckenstein).

0378-7753/$ – see front matter © 2012 Elsevier B.V. All rights reserved.
http://dx.doi.org/10.1016/j.jpowsour.2012.07.144

conductivity in the direction perpendicular to the electrode stack layers of a Li-ion cell have been used – for example 3 W m^{-1} K^{-1}, first determined by Maleki et al. [18]. In other studies Brooman and McCallum [3,4] provided values between 0.87 and 1.26 W m^{-1} K^{-1} for Ni–Cd-cells by considering the individually measured thermal resistances of the differently layers connected in series. This approach is often applied despite neglecting the heat contact resistance between the different layers of the electrode stack. In our recently published work [6] a value of 0.40 W m^{-1} K^{-1} was used that had been identified by cell measurements with internal thermocouples. This discrepancy of nearly one order of magnitude would – in simulation – also lead to a difference of one order of magnitude for the predicted thermal gradient in the cell dependent on the chosen thermal conductivity value. Thus, the thermal characterization of a lithium ion cell is obliged to be considered with similar care as the electrochemical characterization.

This article describes a method of thermal cell characterization as well as the determination of the cell's specific heat capacity and heat conductivity by the Thermal Impedance Spectroscopy (TIS). Additionally, an exemplary application of the TIS on a cylindrical $LiFePO_4$/graphite-cell with a diameter of 32 mm and a cell length of 113 mm is presented, as the cylindrical cell design is identified to be the cell geometry that causes the largest temperature gradients [13]. Detailed information on the used cell is given in Table 1.

2. Conventional methods of thermal characterization

Several previously published articles have examined different methods for determining the anisotropic thermal conductivity properties and the specific heat capacity of battery cells. The specific heat capacity is generally measured in calorimeters [12,18]. Therefore, deep discharged cells are – for example – heated up in a liquid bath inside a dewar vessel and the relation between required energy and temperature rise is observed.

Thermal conductivities for electrode material stacks are measured by different approaches. The most common method is a heat flux measurement. In both works of Maleki and Brooman [3,18] this approach is discussed. Hereby, the main disadvantage is the high measurement and preparation efforts to gain authoritative results. Also the thermal conductivity only of deep discharged specimens cut out of the jelly roll can be determined. Thus, a SoC-dependence of the electrode stack's heat conductivity cannot be examined by this approach.

Further methods of the thermal conductivity determination can be found in literature, such as the Xenon-Flash method by Maleki et al. [18] and the measurement of an operated cell with a cell internal thermocouple by Forgez et al. [7]. Both approaches require also high measurement and preparation efforts. Additionally, the Xenon-Flash-Method can only be operated with deep discharged electrode stacks, as well.

In summary, most of the previously reported methods of thermal characterization are generally extensive, cost-intensive and cell destructive.

A new non-destructive method of thermal characterization of battery cells was firstly described by Barsoukov et al. [1]. In that article the approach of a thermal characterization of a cylindrical Li-ion cell by Thermal Impedance Spectroscopy (TIS) is discussed. The method examines the transfer behavior of the cell surface temperature to the given heat input, inserted on the surface of the battery cell by a heating band wounded around the cell housing. The analysis was executed in the frequency domain.

Recently, Schmidt et al. [22] described an Electro-Thermal Impedance Spectroscopy of a Li-ion pouch cell by using the internal power loss of a battery cell as thermal excitation. As a result, the complex thermal transfer behavior of the pouch cell is characterized in the frequency domain. A main advantage of the TIS by Schmidt is the heat generation being consistent with the thermal situation during cell operation. Thus, a better transferability of measurement results is given. Also, all measurements of this procedure can be operated on a conventional cell test bench expanded only by surface thermocouples as additional test equipment.

This article concentrates on the application of an advanced TIS, also with the internal electrochemical heat excitation, on a battery cell with a more complex geometry (cylindrical cell) that effects higher thermal gradients and thus much bigger differences between surface and maximum jelly roll temperature. In a new approach, the heat excitation can be calculated without the need of previous knowledge of the electrical cell behavior and without using an electrical cell model. Additionally, the focus of this article is laid on the procedure of determining the main thermal parameters of the battery cell, heat conductivity and specific heat capacity, by the TIS in combination with thermal modeling. Finally, a quantitative comparison of TIS-results to values gained by conventional thermal characterization methods is presented.

Table 1
Cell specifications of the investigated Li-ion cell.

Cathode material	$LiFePO_4$	Cell housing diameter	32 mm
Anode material	Graphite	Cell housing length	113 mm
Nominal voltage	3.3 V	Cell weight	194 g
Nominal capacity	4.4 Ah	Can material	Aluminum
Geometrical cell type	Cylindrical		

3. Theory

Impedance spectroscopy is a common tool to examine the transfer behavior of systems in a widely spread field of science. Especially on the sector of battery technology the impedance spectroscopy reached high importance for the analysis of the electrochemical impedance of battery cells at different ambient and load conditions. A main advantage analyzing the frequency spectrum of a system response is the possibility to clearly separate the influences of physical effects with differing time constants that occur simultaneously in the time domain.

The technical procedure of the TIS exhibits several analogies to the electrochemical impedance spectroscopy (EIS). It examines the thermal transfer behavior of a battery cell in the frequency domain compared to the electrochemical transfer behavior in the EIS. EIS determines the electrical impedance $\underline{Z}(j\omega)$, i.e. the transfer function of the voltage response U with respect to the current input I:

$$\underline{Z}(j\omega) = \frac{\underline{U}(j\omega)}{\underline{I}(j\omega)} = Z'(\omega) + jZ''(\omega) \tag{1}$$

with $j\omega = j2\pi f$, where j is the imaginary unit and the f the frequency. $\underline{Z}$ is a complex number, Z' its real part and Z'' its complex part, respectively. $\underline{U}(j\omega)$ and $\underline{I}(j\omega)$ can be derived from the time signals $u(t)$ and $i(t)$ by means of the Fourier transform.

TIS determines the thermal impedance $\underline{G}(j\omega)$, i.e. the transfer function of the temperature response T with respect to the heat generation dQ_{gen}/dt. For the method described here, the heat generation is identical to the power losses in the cell, $dQ_{gen}/dt = P_L$:

$$\underline{G}(j\omega) = \frac{\underline{T}(j\omega)}{\underline{P_L}(j\omega)} = G'(\omega) + jG''(\omega) \tag{2}$$

$\underline{T}(j\omega)$ and $\underline{P_L}(j\omega)$ can as well be derived from the time signals $T(t)$ and $p_L(t)$ by means of the Fourier transform. Apart from these formal analogies there are two important differences:

1. The fundamental time constant of the thermal system is some orders of magnitude higher than that of the electrical system. Roughly, the typical frequency range of EIS is above 1 Hz, the typical frequency range of TIS below 1 Hz.
2. While the electrical current can be both negative and positive, the power loss in a cell is always positive. Consequently the excitation signal p_L is always positively biased.

In both cases, the transfer function of the thermal or electrical equivalent circuit model can be fitted to the measurement results by the variation of the thermal and electrical parameters, respectively. The thermophysical properties of the cell's jelly roll can be calculated from the fitted battery model parameters similar to the electrical properties in the EIS.

One basic principle of the impedance spectroscopy is the Fourier transformation of time discrete signals into the frequency domain by means of the Fast Fourier Transform (FFT). Applying the FFT to the time discrete excitation and response signal, the transfer behavior of the observed system can be examined comparing both frequency spectra.

In analogy to the Fourier transformation, the Laplace transformation is used in this work to describe the transfer behavior of a thermal model as algebraic function $G(s)$ in the frequency domain. Here, s is called the Laplace operator. For the determination of the frequency response characteristic the operator can be substituted by $s = j\cdot\omega$. Similar to the Fourier transformation of the discrete measurement signals, the Laplace transformation enables the frequency spectrum analysis of the generated thermal model. Thus, measurement results and thermal model are compared in the frequency domain using the representation in the complex number plane called Nyquist-diagram.

3.1. Generation of a periodic low-frequency heat source signal

In the described TIS-method, the thermal excitation is realized by the dissipated electrical power loss p_L in the cell's jelly roll. This can be achieved by an amplitude modulated periodic current signal $i(t)$. The composition of the current signal and the resulting power loss are schematically depicted in Fig. 1.

$$i(t) = I(t)\cdot\sin\omega_c t = \hat{i}\cdot\sin\omega_m t\cdot\sin\omega_c t \tag{3}$$

Herein, $\hat{i}$ is the maximum current amplitude of $i(t)$. The carrier frequency $f_c = \omega_c/2\pi$ has to be significantly higher than the modulation frequency $f_m = \omega_m/2\pi$, which has to be in the range of the fundamental frequencies of the device under test. Since the typical thermal time constants of a battery cell are in the range of minutes and thus the modulation frequencies in a range below 100 mHz, this requirement can easily fulfilled with carrier frequencies in the range of 1 Hz or above. The frequency spectrum of such an amplitude modulated signal exhibits two sidebands at $f_c + f_m$ and $f_c - f_m$. The voltage response of a cell with the open circuit voltage OCV and an electrical impedance $\underline{Z}$ is

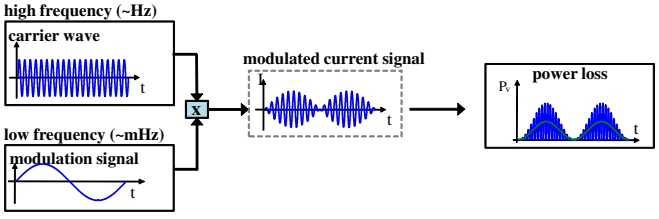

Fig. 1. Schematic process of the generation of an approximately harmonic power loss signal by the modulation of a high frequency carrier signal and a low frequency sine-wave.

$$u(t) = \mathrm{OCV} + \Delta u(t) = \mathrm{OCV} + I(t)\cdot[Z'\sin\omega_c t + Z''\cos\omega_c t] \tag{4}$$

with Z' being the real part and Z'' the imaginary part of the impedance Z at ω_c. The instantaneous power $p(t)$ can be calculated as the product of $i(t)$ and $u(t)$, the resulting term can be written as a function of only $\hat{i}, Z', Z''$ and the frequencies f_c and f_m. The terms of this expression can be sorted to a constant power loss bias $P_{L,avg}$, a power loss at twice the modulation frequency $P_{LM}(2f_m)$ and power losses at higher frequencies at sidebands of the carrier frequency ($f_c \pm f_m$), at twice the carrier frequency ($2f_c$), and at the sidebands of twice the carrier frequency ($2f_c \pm 2f_m$), summarized in P_{LH}.[1] The higher frequency terms contain elements in phase with the excitation and with a phase shift of 90°.

Fig. 2 shows an exemplary spectrum of the power signal calculated via FFT. The phase shifted signals are represented as imaginary numbers.

By means of the FFT the power loss signal at the frequency $2f_m$ can be easily separated from the higher frequency signals and the constant power loss at $f = 0$ Hz. Thus, an input signal for the TIS can be calculated that is purely based on measurements and requires no assumptions on the electrical impedance behavior of the battery cell.

The wanted signal part for the TIS analysis is

$$P_{LM} = -\frac{\hat{i}^2}{4}Z'\cos 2\omega_m t \tag{5}$$

The effective excitation frequency of the TIS therefore is $f_{TIS} = 2f_m$. By varying the modulation frequency f_m for each measurement the thermal impedance spectrum of the cell can be determined. The power loss bias

$$P_{L,avg} = \frac{\hat{i}^2}{4}Z' \tag{6}$$

can be used to determine a thermal *DC-impedance* R_α of the cell surface to the environment, cf. equation (16) in Section 5.

The higher frequency contents P_{LH} are not used in the analysis. For the derivation above a sinusoidal carrier signal was chosen. However, any periodic current signal can be used that is charge neutral and whose fundamental frequency is significantly higher than the modulation frequency. The current and temperature dependency of the electrical cell impedance will lead to a nonlinear distortion, i.e. the resulting power loss signal will not be ideally sinusoidal. Since the nonlinear distortion corresponds to the creation of higher harmonics in the power loss signal, these can be easily removed by use of the Fourier transform.

The current amplitude $\hat{i}$ has to be chosen such that the resulting temperature amplitude is high enough to be measured accurately. If the approximate values of the electrical cell resistance $Z'(\omega_c)$ at the carrier frequency and the thermal impedance $|G|$ at the TIS-frequency f_{TIS} are known beforehand, the excitation current amplitude can be calculated from the desired temperature amplitude ΔT:

$$\hat{i}(f_{TIS}, f_c) = \sqrt{\frac{4\cdot\Delta T}{|G(f_{TIS})|\cdot Z'(f_c)}} \tag{7}$$

4. Experimental and TIS-procedure

The TIS application in this article investigates the thermal transfer behavior between the surface temperature of a cylindrical Li-ion cell (description in Table 1) and the heat generated in the

[1] The frequency doubling can be explained by the square of the current signal and the identity $\sin^2(\omega t) = 1/2(1 - \cos(2\omega t))$.

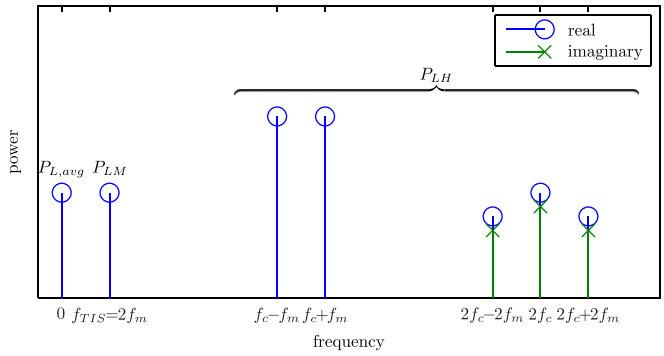

Fig. 2. Schematic power spectrum of a cell with a complex impedance excited by an amplitude modulated current signal.

cell's jelly roll by electrical operation. Two main challenges that are influencing the accuracy of measurement results are discussed in the following two subsections.

4.1. Generation of a one dimensional heat transfer system

In order to deduce the thermal parameters from the later measurement results, a measurement set-up has to be developed that can accurately be reproduced by a preferably simple thermal model. Therefore the thermal heat transfer system – in experiment – should be reduced to a one-dimensionally describable heat transfer problem. The heat flux in three dimensions for using a cylindrical coordinate system with anisotropic heat conductivity can be expressed by Fourier's Law of heat conduction [23]:

$$\frac{1}{\rho c_P}\nabla^2 T + \frac{\dot{q}_q}{\rho c_P} = \frac{\delta T}{\delta t} \tag{8}$$

with

$$\nabla^2 T = \frac{\lambda_r}{r}\frac{\delta}{\delta r}\left(r\frac{\delta T}{\delta r}\right) + \frac{\lambda_\varphi}{r^2}\frac{\delta^2 T}{\delta \varphi^2} + \lambda_z\frac{\delta^2 T}{\delta z^2} \tag{9}$$

Herein, ρ is the material's density, c_P its specific heat capacity, $\dot{q}_q$ the volumetric heat source density, r, φ and z the coordinates of the cylindrical coordinate system and $\lambda_{r,\phi,Z}$ the heat conductivity in each direction.

For the application in this paper, the tangential temperature gradient in equation (8) can be neglected, if the heat transfer coefficient on the surface of the cell can be assumed to be constant. Neglecting the nonlinearity of heat radiation in the temperature region between 10 and 50 °C, an evenly heat transfer coefficient can be achieved by exposing the complete cell housing to natural convection in the climate chamber. Small gradients in local heat transfer coefficients are counterbalanced by sufficient heat conductivity in the aluminum housing.

Within the jelly roll the axial thermal conductivity, which is equivalent to the conductivity parallel to the electrode layers, is in generally by far higher than the cross plane conductivity, as it appears for the jelly roll in radial direction. For example Maleki et al. [18] detected a ratio of in plane to cross plane heat conductivity for a $LiCoO_2$/graphite cell of approx. 9. Gomadam et al. [9] even refer to a ratio of more than 100. The heat flow in axial direction is less limited by the axial heat conduction inside the jelly roll, but is more influenced by the thermal resistances between the jelly roll surface to the terminals on the outside of the cell. These electrical connections are in generally realized by thin strips of metal foils, the extensions of the current collector foils of the electrodes (tabs). As the tabs have only small cross sections perpendicular to the axial heat flux a high thermal resistance occurs. The axial thermal resistances from the jelly roll across the tabs to the battery terminals are in general higher than the radial heat path out of the cell. This can also be seen on the fact, that terminal cooling systems are generally known as less effective than can surface cooling systems [13].

Anyway, for a single cylindrical cell, the axial heat transfer is a non-negligible heat dissipation path. The measurement of the axial heat flow within the terminals is extremely difficult, because they are part of the main electrical current path. As its measurement seems to be not feasible, the axial heat dissipation has to be minimized in order to gain accurate results. Therefore, the most practicable way is to enlarge the experimental setup to three cells connected in series. The applied test setup can schematically be seen in Fig. 3.

All three cells are expected to produce a similar amount of dissipation heat and to possess a similar radial heat transfer coefficient on the can surface. Thus, the cells get heated up during operation to a similar temperature range. In consequence, a falsifying heat flow between the cells is minimized by similar terminal and jelly roll temperatures. The direct mechanical connection of the three cells in series can be understood as the building of two thermal symmetry planes and thus, adiabatic boarders next to the terminals of the inner cell. Additionally, the terminal temperatures of the investigated cell and of the neighboring cell terminals were measured to check the efficiency of the adiabatic walls and to be able to detect an unexpected heat flow between the cells.

By minimizing the axial heat dissipation it can be neglected in the thermal 1D-model discretized only in radial direction. Thus, the Fourier law of heat conductivity for the given one dimensional heat transfer system can be reduced to:

$$\frac{\lambda_r}{\rho c_P}\frac{1}{r}\frac{\delta}{\delta r}\left(r\frac{\delta T}{\delta r}\right) + \frac{\dot{q}_q}{\rho c_P} = \frac{\delta T}{\delta t} \tag{10}$$

4.2. Current excitation signal

For the experimental validation a square wave with a fundamental frequency of 2 Hz was used, which was easier to implement on a conventional test bench than a sinusoidal signal. Moreover, an ideal square wave signal would result in a non-intermitting power loss signal. This benefit is however limited by the maximum current gradient of the test bench.

The amplitude $\hat{i}$ of the carrier wave was pre-configured for each experiment of different frequency by a thermal electrical simulation with a model introduced in Ref. [6] in order to reach a measurable but safe temperature range for the operation of Li-ion cells. This procedure was repeated for all tests shown in Table 2 with varying frequency and adapted maximal current factor. The test was operated on the experimental setup of Fig. 3 connected to a battery test bench. The surface temperature of the investigated cell housing was measured by temperature sensors (TC) 1, 2 and 6. The housing temperature of the two outer cells were measured by TC 10 and 11, the terminal temperatures were measured by TC 3, 5, 7 and 9.

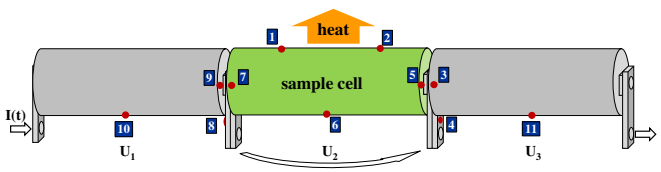

Fig. 3. Experimental setup of the applied TIS on three serial connected cylindrical $LiFePO_4$-cells and numerated thermocouples.

Table 2
Test-matrix with 12 applied sequences of different frequencies.

Sequence	1	2	3	4	5	6	7	8	9	10	11	12
f_{TIS} (mHz)	50	30	10	7	5	3	1	0.8	0.6	0.4	0.2	0.1
$\hat{i}$ (A)	104	102	99	96	94	92	90	88	83	76	74	72

5. Modeling

In order to obtain the thermal parameters radial heat conductivity λ_r and specific heat capacity c_P from the measured thermal characterization a thermal model has to be developed. These thermal parameters are later varied in a mathematical least distance fitting algorithm in the Nyquist plot to adapt the model transfer behavior to the measurement results. The Fourier law for one dimensional heat flux described by equation (10) in radial direction of the Li-ion cell was discretized by the use of the Finite-Volume-Method. For model simplification c_P, λ_r and the density ρ of the jelly roll is assumed to be homogenous. The jelly roll is modeled as a hollow cylinder enclosed by an additional heat capacity of the cell housing on the outer surface of the jelly roll. On the outer cell housing surface a constant heat transfer coefficient to the environment is assumed. The thermal inertia of the surface thermocouples was modeled by an additionally thermal PT_1-element, representing the thermal capacity of the sensor and the thermal resistance from the cell housing across the electrically isolating Kapton-foil to the sensor head.

A one-dimensional heat flux modeled by Finite Volume elements discretized in time by an explicit Euler method can be described by the energy balance for an element E:

$$C_E\left(T_E^{(2)}-T_E^{(1)}\right)=\left(P_{\mathrm{L}}\frac{V_E}{V_{\mathrm{tot}}}+\frac{T_{E+1}^{(1)}-T_E^{(1)}}{R_{\mathrm{th},E\to E+1}}-\frac{T_E^{(1)}-T_{E+1}^{(1)}}{R_{\mathrm{th},E-1\to E}}\right)\Delta t \tag{11}$$

with V_{tot} being the total jelly roll's volume and ΔT the time step. For the discrete energy balance applied in radial direction of the jelly roll, the thermal capacity C_E and the thermal resistance R_{th} of the finite element to neighboring elements can be determined by equations (12) and (13).

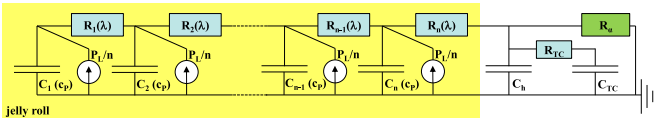

Fig. 4. 1D-thermal model spatialized in radial direction for the test setup with a cylindrical Li-ion cell.

$$C_E = \left(r_{\mathrm{o},E}-r_{\mathrm{i},E}\right)^2\pi\rho c_P L \tag{12}$$

and

$$R_{\mathrm{th},E\to E+1} = \frac{\ln\frac{r_{\mathrm{c},E+1}}{r_{\mathrm{c},E}}}{\lambda_r 2\pi L} \tag{13}$$

where $r_{\mathrm{o},E}$, $r_{\mathrm{i},E}$, $r_{\mathrm{c},E}$ are the element's outer, inner and centroid radius and L its length in z-direction. Applying the energy balance of equation (11) for all radial elements (index 1 to n), a thermal one dimensional Finite Volume Model can be assembled, as depicted in Fig. 4.

Herein the thermal capacities are represented in electrical analogy as a capacity against ground (ambient temperature) connected by thermal resistances. The generated power loss has to be distributed homogenously across the finite volumes that represent the electrode stack. The number of finite volumes representing the jelly roll in the model was varied between one and six elements expecting a converging behavior of the fitted parameter values. The transfer function $G_{\mathrm{model}}(s)$ of the housing surface temperature in dependence of power loss excitation for the model with n finite jelly roll volume elements can be deduced by the solution of the system of differential equation described in the frequency domain in equation (14).
with

$$\begin{pmatrix}
1 & 1 & & & & \ddots & & & & & & & & \ddots & \ddots \\
 & -1 & 1 & 1 & & \ddots & & & & & & & & \ddots & \ddots \\
 & & & -1 & 1 & \ddots & \ddots & \ddots & \ddots & \ddots & \ddots & & \ddots & \ddots & \\
 & & & & & \ddots & & -1 & 1 & 1 & & & & & \\
\frac{1}{C_1\cdot s} & -R_1 & -\frac{1}{C_2\cdot s} & & & \ddots & & & & -1 & 1 & & 1 & 1 & \\
 & & \frac{1}{C_2\cdot s} & -R_2 & -\frac{1}{C_3\cdot s} & \ddots & & & & & & & & & \\
 & & & & & \ddots & \ddots & \ddots & \ddots & \ddots & \ddots & & \ddots & \ddots & \\
 & & & & & \ddots & \frac{1}{C_{n-1}\cdot s} & -R_{n-1} & -\frac{1}{C_n\cdot s} & & & & & & \\
 & & & & & \ddots & & & \frac{1}{C_n\cdot s} & -R_n & -\frac{1}{C_h\cdot s} & & & & \\
 & & & & & \ddots & & & & & \frac{1}{C_h\cdot s} & -R_{\mathrm{TC}} & -\frac{1}{C_{\mathrm{TC}}\cdot s} & & \\
 & & & & & \ddots & & & & & \frac{1}{C_h\cdot s} & & & R_\alpha &
\end{pmatrix}
\cdot
\begin{pmatrix}
\dot{Q}_{C_1}\\ \dot{Q}_{R_1}\\ \dot{Q}_{C_2}\\ \dot{Q}_{R_2}\\ \dot{Q}_{C_3}\\ \vdots\\ \dot{Q}_{C_{n-1}}\\ \dot{Q}_{R_{n-1}}\\ \dot{Q}_{C_n}\\ \dot{Q}_{R_n}\\ \dot{Q}_{C_h}\\ \dot{Q}_{\mathrm{TC}}\\ \dot{Q}_\alpha
\end{pmatrix}
=
\begin{pmatrix}
\frac{P_V}{n}\\ \frac{P_V}{n}\\ \frac{P_V}{n}\\ \vdots\\ \frac{P_V}{n}\\ 0\\ 0\\ \vdots\\ 0\\ 0\\ 0\\ 0
\end{pmatrix} \tag{14}$$

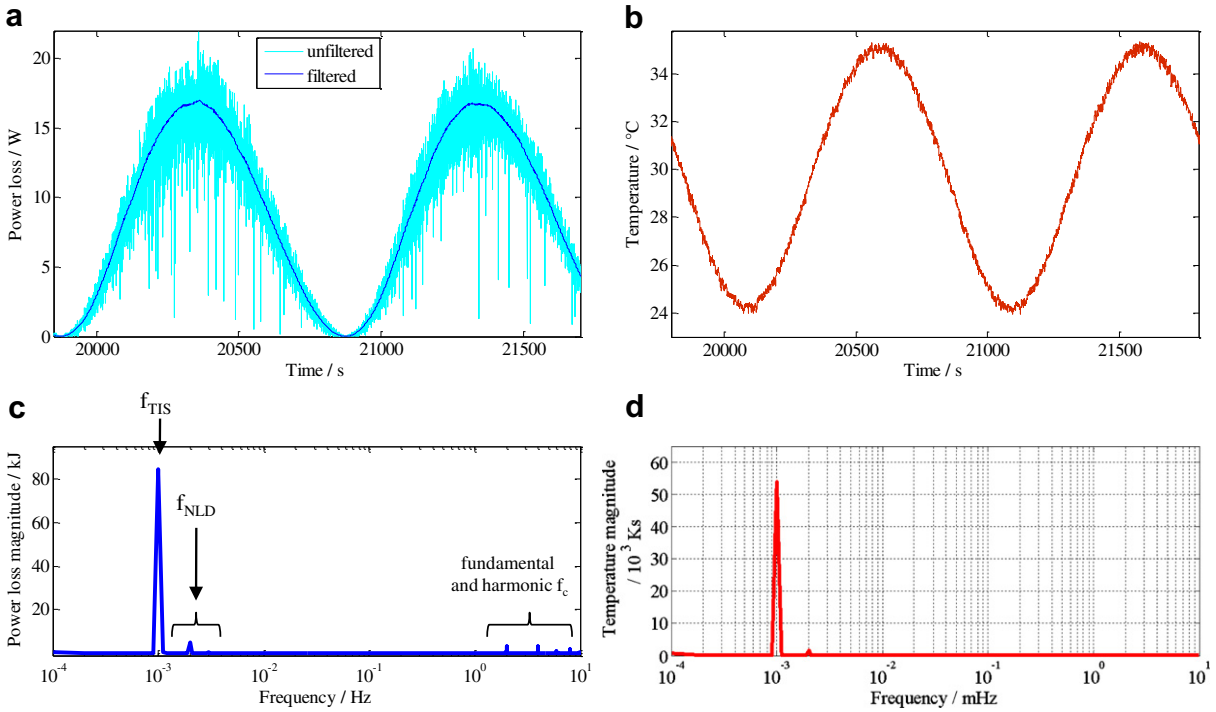

Fig. 5. Cell's power loss as thermal excitation for 1 mHz-test in the time domain (a) and the frequency domain (c); Cells surface temperature as system response in the time domain (b) and the frequency domain (d).

$$T_{TC} = \frac{\dot{Q}_{TC}}{C_{TC} \cdot s} \tag{15}$$

The determination of transfer functions for models of more than two finite elements was solved by Matlab symbolic toolbox. Although the number of thermal resistances and capacities grows with the number of finite volumes, the degree of freedom remains constant as all model parameters of the jelly roll are – beside geometry – only dependent on $p_L = \Delta u(t) \cdot i(t)$ and λ_r.

Thus, the behavior of the overall thermal model are defined by five parameters: (1) λ_r of the jelly roll, (2) c_P of the jelly roll, (3) total heat capacity of the cell housing C_h, (4) convective heat transfer coefficient on the cell's surface α and (5) the thermal time delay of the electrically isolated thermocouple $T_{0,TC}$.

The mean difference between surface and ambient temperature $T_{S,avg} - T_{amb}$ in the thermal quasi-steady state was used for the calculation of the heat transfer coefficient α and the corresponding convective resistance R_α, as shown in equation (16).

$$R_\alpha = \frac{1}{\alpha \cdot A_S} = \frac{T_{S,avg} - T_{amb}}{P_{L,avg}} \tag{16}$$

with A_S being the cell surface area and $P_{L,avg}$ the cell's average power loss. Furthermore, the thermal time delay of the electrically isolated surface temperature sensor was determined in preliminary tests exposing a nonisolated as well as with Kapton foil isolated thermocouple to a nearly ideal temperature step. Extracting the additional time constant of the electrical isolation and adding it to the time delay of the thermocouple specification, a thermal time delay of $T_{0,TC} = 2.9$ s could be determined. Consequently only three fitting parameters of the thermal model namely λ_r, c_P and C_h had to be varied to fit the thermal model behavior to the measurement results.

6. Results

For each frequency listed in Table 2 the cell surface temperature (average value of sensor 1, 2 and 6), current flow and voltage response of the investigated cell were monitored for several oscillation periods at a sample frequency of 20 Hz. Only oscillations in a thermal quasi steady state, for which the temperatures at the beginning of each wave are constant, were included in the frequency domain analysis. The power loss of the investigated cell was calculated by $p_L = \Delta u(t) \cdot i(t)$. For $f_{TIS} = 1$ mHz an extract of the calculated power loss is illustrated in Fig. 5a (light blue line) (in the web version). This signal seems to be a periodic harmonic low-frequency wave superposed by a high frequency noise signal. The noise signal is the result on the one hand of the electrochemical impedance asymmetry [5] between charging and discharging and on the other hand of the finite current rate gradient during the change of current direction. Here, some values of the voltage signal were recorded while the test bench switched the current direction. For a better demonstration the p_L-signal is also illustrated filtered by a centered moving 25 s-average filter (dark blue line) (in the web version).

An extract of the surface temperature during thermal quasi-steady state for 1 mHz-excitation can be seen in Fig. 5b. For the analysis in the frequency domain the steady state oscillations (at least two full oscillations per frequency) were cut out from temperature and power loss signals and transferred into the frequency domain by a Fast Fourier Transformation using Matlab. Fig. 5c and d shows the amplitude spectra vs. frequency of both signals for 1 mHz-excitation. Herein, the magnitudes of both signals have their clear maxima at the low frequency of the excitation current signal. Further peaks at multiples of the power loss frequency show the small but detectable influence of non-linearities in both, the power loss generation and the observed thermal system (compare to f_{NLD} in Fig. 5c). Also small maximas can be detected at the fundamental and harmonic frequencies of the

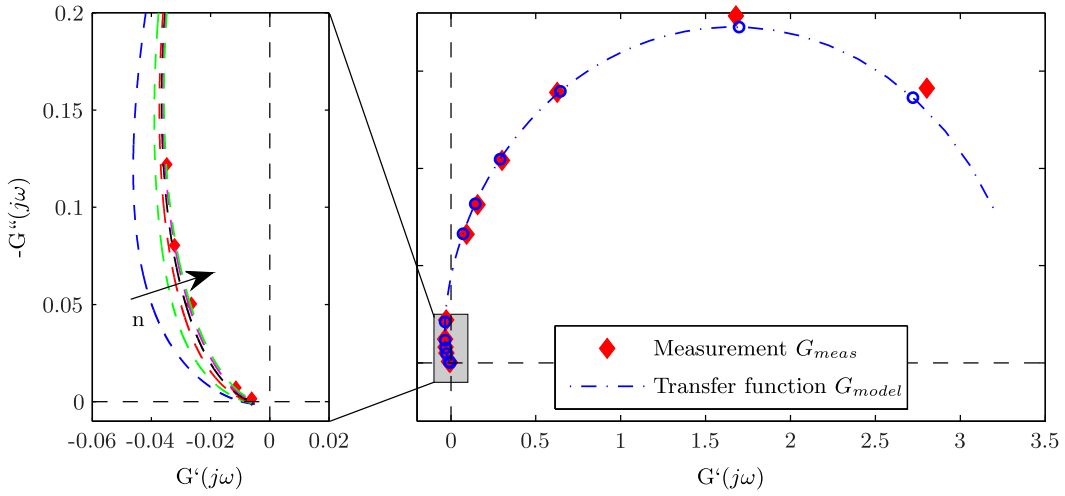

Fig. 6. Nyquist plot of the TIS application; comparison of the fitted model transfer function (line) to the measurement results (red squares) in the complex time domain; *right*: whole frequency range; *left*: high frequency range. (For interpretation of the references to colour in this figure legend, the reader is referred to the web version of this article.)

carrier signal. The ratio of the amplitude of both spectra at 1 mHz in combination with the phase displacement between temperature and power loss signal defines a single point in the complex time plane, called thermal impedance $G_{meas}(f_{TIS})$. For all twelve operated tests with different frequencies the Nyquist plot can be seen in Fig. 6 (red squares).

In order to detect the thermal parameters λ_r, c_P and C_h in the experiment the transfer function of the thermal model in the frequency domain was fitted to the measured Nyquist plot in the complex plane using the Matlab function *fminsearch*. Inside the optimization algorithm the chosen residuum to be minimized was defined as the sum of square distance between the measurement point in the complex plane and the thermal impedance point of the transfer function at the same frequency. It can be calculated using equation (17):

$$\mathrm{Res}_{\min} = \sum_{i=1}^{n}\Big(\left(G'_{\mathrm{meas}}(f_i) - G'_{\mathrm{model}}(f_i)\right)^2 + \left(G'_{\mathrm{meas}}(f_i) - G'_{\mathrm{model}}(f_i)\right)^2\Big) \quad (17)$$

Fig. 6 shows also the comparison between measurement results and the fitted thermal model. Herein the blue dashed line represents the Nyquist-curve of the thermal model with six control volumes. The small blue cycles depicts the thermal impedance of the model only for the twelve observed testing frequencies in comparison to the measurement results (red squares). A good accordance between measurement and fitted model can be seen at nearly all test frequencies. A significant deviation between measured and fitted thermal impedance can only be detected for the lowest frequency (0.1 mHz). Therefore, one possible explanation could be the higher surface temperature differences in one testing period and additionally the changing air circulation in the climate chamber over the long measurement duration.

By comparing the fitting results with different degrees of spatial resolution (growing n in Fig. 4) no significant discrepancy at lower frequencies can be seen, whereas at higher frequencies differing Nyquist plots are observed. Fig. 6 (left) shows that for these frequencies with growing number of control volumes in the thermal model the phase delay, which is higher than $\pi/2$ for the test frequencies above 1 mHz, shrinks. Additionally the transfer functions of the thermal models graphically converge to the measured thermal impedances with growing control volumes.

Table 3 compares the fitted parameters of the different thermal models. Therefore, the overall specific heat capacity was calculated by the sum of housing and jelly roll capacity divided by the cell weight. The thermal parameters in Table 3 deduced from the fitting algorithm also show the variation of the parameter results between the three measurement with the same test setup (V1, V2 and V3, operated in time intervals of several days) of less than ±1% for the specific heat capacity and about ±4% for the heat conductivity. These variances are indicators for the good reproducibility of the measurement method according to the influence of measurement errors, environmental system errors and model fitting inaccuracies.

The forth test series (V4) is a TIS operated on an equal test setup with a replaced inner test cell. This test was executed in order to evaluate the reproducibility of the results according to tolerances of the thermocouples and to tolerances in the test setup, but also according to cell production variances. The results extracted from the test series V4 exhibit a deviation from the mean values of V1 to V3 of 5% for the specific heat capacity and only about 1% for the thermal conductivity.

With increasing complexity of the thermal model a convergence of both thermal parameters – c_P and λ_r – can be detected. This is

Table 3
Fitted thermal parameters of different discretized thermal models on measurement results. V1–V3 are repeated measurements on the test setup. V4 was the same test procedure with switched cells.

	Specific heat capacity (J kg^{-1} K^{-1})				Radial heat conductivity (W m^{-1} K^{-1})			
	V1	V2	V3	V4	V1	V2	V3	V4
1 CV	1080.0	1028.1	1030.8	1116.4	1.09	0.77	0.79	0.87
2 CV	1049.6	1049.7	1033.9	1083.6	0.67	0.67	0.61	0.58
3 CV	999.0	1009.1	996.1	1044.5	0.45	0.48	0.45	0.44
4 CV	975.4	988.2	977.3	1026.5	0.38	0.41	0.39	0.38
5 CV	963.4	977.3	967.6	1017.6	0.36	0.38	0.37	0.36
6 CV	956.8	971.0	961.9	1012.2	0.34	0.37	0.35	0.35

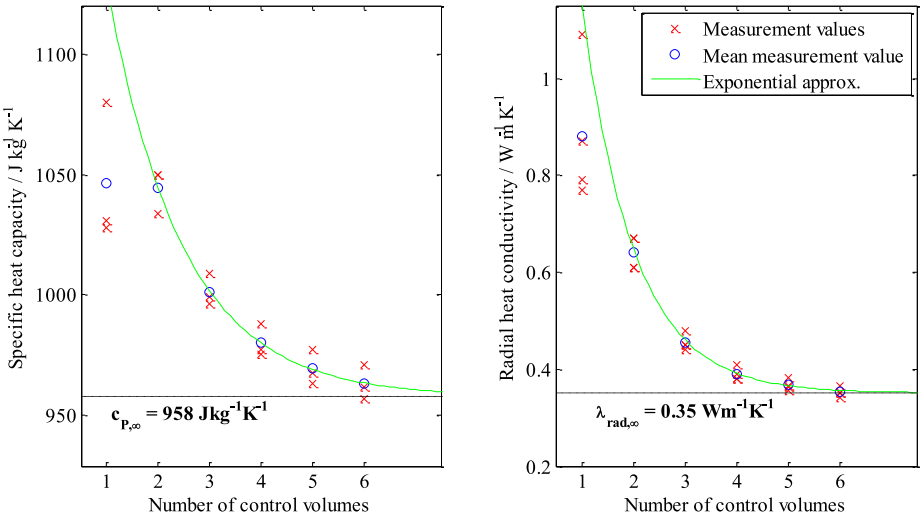

Fig. 7. Fitted thermal parameters for different numbers of control volumes in the thermal model and the converging parameter values for eliminated discretization error, *left*: specific heat capacity of cell, *right*: radial heat conductivity of the jelly roll.

also demonstrated in Fig. 7. Herein the virtual boundary values for both parameters are depicted assuming an exponentially decreasing discretization error with increasing number of control volumes. For the calculation of the extrapolation curves, the mean fitted thermal parameter of measurement 1–3 – for the models with more than one control volume of the jelly roll – were used.

7. Discussion

In order to receive indications on the accuracy of the exemplary TIS application a cell of the same type has previously be examined in accurate, complex and destructive thermal characterization procedures at the Fraunhofer Institute of Chemical Technology (ICT) in Karlsruhe.

The cell's overall specific heat capacity was accurately determined via temperature rise analysis in a calorimeter comparable to Ref. [12] and was calculated to 1020 J kg^{-1} K^{-1}. Approximately the value determined in the TIS is reduced by 5% compared to the reference characterization test in the calorimeter. The difference in the results of the two characterization methods can be explained by the thermal heat capacity of the cell terminals. These capacities are thermally connected to the jelly roll only by – compared to the inside of the jelly roll – high thermal resistances through the current collector tabs. Additionally at least the anode terminal is thermally poorly connected to the cell housing by an electrical insulation. Thus, both terminals are partially thermally separated from the main cell components. As a consequence the TIS analysis with a thermal 1D-model that does not include the cell terminals will result in a reduced measured c_P-value underestimating the thermal capacity of the cell terminals. If this measurement error is not considered and eliminated in the analysis procedure, the difference can be seen as the inaccuracy of the determination of c_P by the TIS.

In future investigations, the two terminals can be considered by the use of two more thermal masses in the thermal model. This can help to further reduce the inaccuracy of both, the heat capacity and the heat conductivity measurement, although the determination of a SISO-transfer function will be significantly complicated.

Secondary, λ_r was determined at the ICT by means of heat flux measurements. Herein, heat was inserted via a resistive heater on the surface of a deep discharged and extracted jelly roll. The inner core of the cell was replaced by a cooling element. Considering the geometrical conditions of the experiment, the radial thermal conductivity was calculated via the temperature difference from outer to inner jelly roll surface to 0.40 W m^{-1} K^{-1}. Comparing the value determined in the TIS of 0.35 W m^{-1} K^{-1} to the reference measurement a relative difference of 12% can be identified.

Predominantly, the discrepancy between the two measurement procedures has to be attributed to the measurement inaccuracy of both methods, the non-destructive as well as the destructive method.

Further on, special attention should be paid on a possible physical reason for the discrepancy between the two methods. The two procedures rely on basically different electrochemical conditions of the jelly roll during the experiments.

In the TIS the jelly roll is operated at a SoC of 50%. In contrast, the heat flux measurements were done on a deep discharged jelly roll (<0% operating SoC). As the graphite anode possesses a definitely higher electrical conductivity than the $LiFePO_4$-cathode, also for thermal consideration, the cathode seems to influence the thermal resistance perpendicular to the electrode stack in a higher degree. According to Ref. [3], the thermal conductivity of electrode materials can rise with the amount of intercalated metallic atoms. As the cathode of Li-Ion-Cells is fully intercalated by Li-ions in the deep-discharged state, the cathode material – the bottle neck of heat conduction perpendicular to the electrode stack – will possess better heat transfer behavior at low SoCs. Thus the difference of λ_r measured by the two methods – TIS and heat flux measurement – could also be caused by different SoCs during the characterization methods.

If this effect would significantly influence the measurement results, a definite advantage of the TIS as measurement procedure for thermal conductivity could be seen: By using the TIS, a Li-Ion cell can be investigated in the real operating range of an electrical energy storage (0% < SoC < 100%). In contrast, all destructive methods of conductivity measurements can only be operated on deep discharged jelly rolls or even segments cut out of these. The real influence of this effect can be evaluated in future quantitatively by applying the TIS at different states of charge.

8. Conclusion and future aspects

This article describes the application of an alternative to conventional methods for the thermal characterization of battery

cells, the Thermal Impedance Spectroscopy on a cylindrical Li-ion cell. Therefore, a battery cell test set-up was defined that could be exactly thermally described by a simple 1D thermal model. A periodic low frequency power loss signal was generated inside the jelly roll of the battery cell via a modulated current signal. The power loss signal could be calculated using the measured current and voltage profiles without the need of any previous knowledge of the electrical cell behavior. The transfer behavior of the temperature response on the cell's surface to the power loss excitation was analyzed in the frequency domain. The transfer function of a thermal model representing the thermal heat flux problem of the experiment was developed and it's parameters, specific heat capacity and thermal conductivity, were determined by fitting the model to the measurements in the Nyquist plot. Compared to conventional thermal characterization methods the TIS showed good agreement of results for the specific heat capacity. A possible explanation for the relative difference of 12% in the thermal conductivity determination could be the measurement conditions that are closer to real life operation for the TIS method. Consequently, a main portion of the deviation could be attributed to the difference of the heat conductivity of a deep discharged jelly roll (as investigated in the conventional method) and the jelly roll in a regular operation range (as investigated in the TIS). Following, there are indication that the inaccuracy of the exemplary operated TIS is even less than 12%.

One future aspect of the TIS will be the reduction of measurement time. For example a cooling fan could downsize the convective resistance on the surface and thus the system time constant reducing the test time effort significantly. Additionally, pre-measurement time could seriously be shortened by using a direct power loss control on the battery test bench described by the patent of Bohlen [2].

In order to improve the TIS accuracy, the inertia of the thermocouples could be reduced by using high dynamical temperature sensors that are thermally better connected to the cell can surface. This would lead to a decreased influence of the sensor time constant on the measurement results and especially, to a decreased influence of errors in the time constant determination on the results.

Finally the amplification of the method to a multi dimensional TIS will be a challenging subsequent work for determining the heat conductivity in several directions of the jelly roll by the application of SIMO-system analysis (Single Input, Multiple Output).

As the TIS is an easy to operate method, its application on cells embedded in cell modules or even in whole energy storage systems can in future be implemented in battery control units for onboard thermal characterization during operation.

Anyway, the TIS can be described in summary as a practicable and also accurate method combining the determination of specific heat capacity and heat conductivity in one measurement. Thus, the TIS replaces two destructive and extensive experimental methods by one non-destructive method, that enables the thermal characterization of a battery cell during operation conditions on a conventional battery test bench only expanded by temperature measurement equipment on the cell surface.

References

[1] E. Barsoukov, J.H. Jang, H. Lee, Journal of Power Sources 109 (2002) 313–320.
[2] O. Bohlen, German patent DE102009037085a1: Ermittlung einer Verlustleistung eines Energiespeichers, 2011.
[3] E.W. Brooman, J. McCallum, Journal of the Electrochemical Society 118 (1971) 1518–1523.
[4] E.W. Brooman, J. McCallum, Journal of the Electrochemical Society 119 (1972) 1137–1141.
[5] S. Buller, 2002. Impedance-based simulation models for energy storage devices in advanced automotive power systems. Phd thesis, RWTH Aachen University.
[6] M. Fleckenstein, O. Bohlen, M.A. Roscher, B. Bäker, Journal of Power Sources 196 (2011) 4769–4778.
[7] C. Forgez, D.V. Do, G. Friedrich, M. Morcrette, C. Delacourt, Journal of Power Sources 195 (2010) 2961–2968.
[8] J. Gerschler, J. Kowal, M. Sander, D.U. Sauer, in: Electric Vehicle Symposium (EVS 23), Anaheim, 2nd–5th December, 2007.
[9] P.M. Gomadam, R.E. White, J.W. Weidner, Journal of the Electrochemical Society 150 (10) (2003) A1339–A1345.
[10] W.B. Gu, C.Y. Wang, Journal of the Electrochemical Society 147 (2000) 2910–2922.
[11] G. Guo, B. Long, B. Cheng, S. Zhou, P. Xu, B. Cao, Journal of Power Sources 195 (2010) 2393–2398.
[12] J. Harmel, 2005. Betrachtungen zur Wärmebilanz von Nickel-Metall-Hydrid Batterien. Ph.D. thesis, TU Dresden.
[13] T. Heckenberger, D. Neumeister, A. Wiebelt, H.-G. Herrmann, C. Fehrenbacher, T. Isermeyer, in: 9. Internationales Stuttgarter Symposium, Automobil- und Motorentechnik, Stuttgart, 24th–25th March, 2009.
[14] S.A. Khateeb, S. Amiruddin, M. Farid, J.R. Selman, S. Al-Hallaj, Journal of Power Sources 142 (2005) 345–353.
[15] G.-H. Kim, A. Pesaran, R. Spotnitz, Journal of Power Sources 170 (2007) 476–489.
[16] R. Kizilel, R. Sabbah, J.R. Selman, S. Al-Hallaj, Journal of Power Sources 194 (2009) 1105–1112.
[17] D. Linzen, 2006. Impedance-based loss calculation and thermal modeling of electrochemical energy storage devices for design considerations of automotive power systems. Phd thesis, RWTH Aachen University.
[18] H. Maleki, S.A. Hallaj, J.R. Selman, R.B. Dinwiddie, H. Wang, Journal of the Electrochemical Society 146 (1999) 947–954.
[19] H. Maleki, A.K. Shamsuri, Journal of Power Sources 115 (2003) 131–136.
[20] R. Sabbah, R. Kizilel, J. Selman, S. Al-Hallaj, Journal of Power Sources 182 (2008) 630–638.
[21] J.P. Schmidt, T. Chrobak, M. Ender, J. Illig, D. Klotz, E. Ivers-Tiffee, Journal of Power Sources 196 (2011) 5342–5348.
[22] J.P. Schmidt, D. Manka, D. Klotz, E. Ivers-Tiffee, Journal of Power Sources 196 (2011) 8140–8146.
[23] K. Stephan, F. Mayinger, Thermodynamik – Band1: Einstoffsysteme. Grundlagen und Technische Anwendungen, fifteenth ed., Springer-Verlag Berlin, 1998.